THE EFFECT OF SURFACTANT SOLUTIONS ON FLOW STRUCTURES IN TURBULENT RAYLEIGH-BENARD CONVECTION

by

Tongzhou WEI[a], Weihua CAI[a,*], Changye HUANG[a], Hongna ZHANG[a,*], Wentao SU[b], and Fengchen LI[a]

[a] School of Energy Science and Engineering, Harbin Institute of Technology, Harbin, China
[b] School of Energy and Power, Shenyang Institute of Engineering, Shenyang, China

Original scientific paper
https://doi.org/10.2298/TSCI171026263W

This paper presents an experimental study on the flow structures in turbulent Rayleigh-Benard convection with surfactant solutions. The shadowgraph visualization was used to obtain the plumes and the velocity field was measured using particle image velocimetry. The results show that the size of plumes in surfactant solution case is larger than that in Newtonian fluid case and it needs more time for surfactant solution case to start convection. The large-scale circulation fails to form in surfactant solution case and the convection velocity is smaller. A decrease of the measured Nusselt number is observed in surfactant solution case. The phenomena are caused by the shear-shinning and elastic characteristics of surfactant solution.

Key words: *surfactant solutions, Rayleigh-Benard convection, thermal plumes, large-scale circulation*

Introduction

Nowadays, new renewable energy has been widely developed, and heat transfer is an important issue using these energy sources. Turbulent thermal convection usually exists in many engineering applications, where heat transfers are involved, such as nuclear reactors, solar heat exchanger, and energy storage. A classical model for turbulent thermal convection is Rayleigh-Benard convection (RBC). It describes a cell filled with fluid heating from the bottom and cooling on the top. The RBC system is an idealized model to study turbulent flows involving heat transport and has attracted much attention during the past few decades [1].

For a RBC system, it only has two controlling parameters: Rayleigh number and Prandtl number. There exist two kinds of flow structures in RBC: plumes and large-scale circulation (LSC). Now, much attention has been paid to plumes and LSC. The studies show that there are two kinds of plumes: mushroom like plumes and sheet like plumes [2, 3], which can transmute into each other [4] and they play an important role in heat transport. Shang *et al*. [5, 6] simultaneously measured local velocity and temperature to calculate the heat flux in the central region and the sidewall region. It was found that the heat flux in the convection

* Corresponding authors, e-mail: caiwh@hit.edu.cn; zhanghn@hit.edu.cn

cell was mainly transported by plumes along the sidewall of convection cell. The same conclusion have been obtained in the experiments of Gasteuil *et al*. [7] Kaczorowski and Wanger [8] used direct numerical simulation (DNS) to study the relationship between temperature dissipation rate inside plumes and heat transfer. The results also showed the important role of plumes on heat transfer in RBC. Zhou and Xia [9] studied the density of plumes and found that the number of plumes increased with the increase of Rayleigh number, and the scaling law for the number of plumes was the same as that for Nusselt number. It was indicated that the heat carried by a single plume was constant in the same RBC system, and the increase of Nusselt number was mainly due to the increase in the number of plumes. The LSC has been known as the *mean wind* in RBC. This phenomenon was firstly discovered by Krishnamurti and Howard [10]. The experiments of Qiu *et al*. [11] also confirmed that LSC was similar to a *flywheel* structure. Xi *et al*. [12] demonstrated that the dynamical origin of the initial horizontal motion required by LSC stemmed from the movement of plumes. As a coherent large-scale structure, LSC also has many intriguing dynamic features, such as azimuthal rotation, cessation and reversal. The angular motion of LSC was generally similar to the Brownian motion [13]. Cessation means the sudden loss of turbulent intensity in LSC and reversal represents LSC to move in the opposite direction. Brown *et al*. [14] found that LSC may flow in any direction after cessation, that is to say, reversal is only a special case of cessations. Based on the experimental results, Xi and Xia [15, 16] found that the cessation was more likely to occur after the reversal.

In recent years, there are many researches focusing on RBC with Newtonian fluids, while the studies on RBC with viscoelastic fluids are just the beginning. A heat transport experiment was firstly conducted in a RBC system with polymer solutions (one classical kind of viscoelastic fluids) [17]. It was found that a monotonic decrease of Nusselt number with the increasing polymer concentration. However, based on DNS studies, it has been shown that it is possible to achieve an increase for Nusselt number in bulk turbulent thermal convection with polymer solutions [18]. Through the experimental results, Wei *et al*. [19] have found an increase of Nusselt number beyond certain polymer concentration in RBC with by using rough plates, but the addition of polymers could reduce the heat transfer in RBC with smooth plates. The similar results of enhancing and reducing heat transfer can be also obtained by DNS [20, 21]. Recently, Chen *et al*. [22] found that the addition of polymers reduced the heat flux and the amount of heat transfer reduction behaves non-monotonically, which firstly increases but then decreases with Weissenberg number. From the previous investigations, it can be clearly seen that the influence of polymer additives have remarkable influence on RBC. However, it is still unknown whether there exists the influence of surfactant solution (another classical kind of viscoelastic fluids) on RBC. No attention has been paid to this topic. Therefore, in order to investigate the effect of surfactant solution on flow structures (plumes and LSC) in RBC, we carried out the experiments using the shadowgraph visualization and particle image velocimetry (PIV) techniques.

Experimental set-up and measurement methods

Experimental set-up

The experiments were carried out in a square convection cell, as shown in fig. 1, which included sidewall, top plate, bottom plate, heater, thermistors, and so on. The sidewall is made of Plexiglas, which had the low thermal conductivity to effectively reduce heat transfer into the environment. Two convection cells with different sizes were used in the experi-

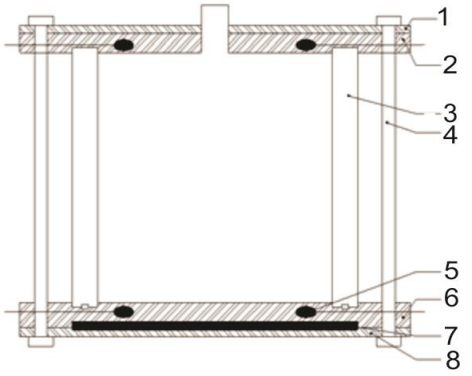

Figure 1. Schematic diagram of the convection cell used in the experiment; *1 – upper cover plate, 2 – upper plate, 3 – Plexiglas side wall, 4 – steel post, 5 – thermistor, 6 – lower plate, 7 – electric heater, and 8 – lower cover plate*

ments: one used in the shadowgraph experiment with the height, length and width of 220 × 220 × 220 mm, the other used in the PIV measurement with the height, length and width of 150 × 150 × 150 mm. The aspect ratio of both convection cells is 1.0 (aspect ratio is defined as the ratio of the height to the width).

The top and bottom plates were made of Cu, which had high thermal conductivity to ensure the temperature in both plates keeping uniform. Two channels were machined on the top surface of upper plate, which was connected with a water cooler to cool the top plate. The bottom plate was connected to an electric heater, and the heater power was controlled by a power supply. On the surface of either top or bottom plate, a thin-layer of gold film was coated to provide a smooth boundary and prevent the oxidation of plate. Four steel posts were inserted between top plate and bottom plate to hold the convection cell together. The temperature difference across the cell was measured by thermistors imbedded in the plates.

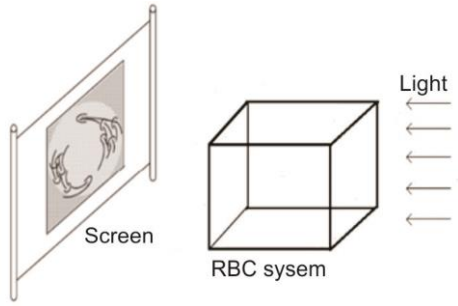

Figure 2. Schematic diagram of the shadowgraph visualization

Measurement methods

The shadowgraph visualization is one kind of methods to obtain the shapes of plumes and the flow states of LSC. Its basic principle is: let the light pass through the RBC system, when thermal convection occurs in the cell, the refractive index of liquid can change, which causes the shadow image to change. So the images of plumes can be presented on the screen. Figure 2 shows a schematic diagram for the shadowgraph visualization of plumes. A uniform and collimated beam of white light from an astral lamp is shone through the cell. On the other side of the cell, the shadowgraph is observed on the screen and is captured by a CCD camera. Through this experiment, it can record the shadowgraph of flow structures during the beginning to the steady-state of convection. Experimental procedure of the shadowgraph visualization was: At the initial state, the temperature of convection cell was kept at 20 °C. The electric heater began to heat the bottom plate with a constant power until the temperature of bottom plate reaches 40 °C. Meanwhile, the temperature of top plate was kept at 20 °C. Then it made the system enter into a steady-state by regulating power. It needed about one hour for bottom plate to reach 40 °C and needed additional three hours to reach the steady-flow. The camera recorded the image of flow structures at the starting state and the steady-state.

We used a 2D-PIV to measure the instantaneous velocity field at the middle plane of convection cell, as shown in fig. 3. It needed three hours to reach the steady-state and then the velocity field was measured. Some parameters of the key components in the PIV system were introduced: the double-pulsed Nd-YAG (YAG-yttrium aluminum garnet) lasers with an output

of 200 mJ/pulse and the trigger rate of 5 Hz, the CCD camera (FlowSense 4M EO Model81C92) with a resolution of 2048 × 2048 pixels. The seeding particles were hollow glass spheres with typical diameter of the order ≤20 μm. The PIV image covered an area of about $x \times y = = 180 \times 180$ mm^2. Here, the area of PIV image was larger than the size of the experimental set-up so as to obtain the whole flow field in the convection cell. The interrogation area was set to be 64 × 64 pixels (with 50% overlap in each direction). The spacing between adjacent vectors in each direction was around $\Delta x = 3$ mm and $\Delta y = 3$ mm.

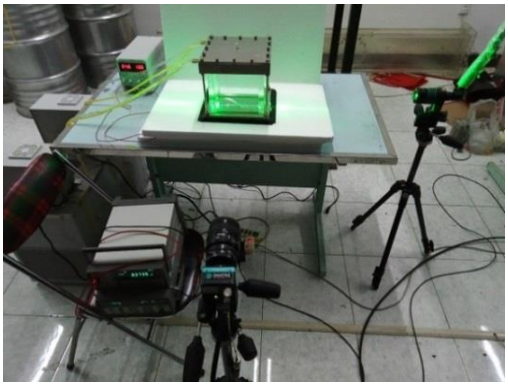

Figure 3. The photo of RBC system based on PIV measurement

Viscosity measurement of surfactant solution

The cetyltrimethyl ammonium chloride (CTAC) was used as surfactant additive and sodium salicylate (NaSal) was applied to provide the counter ions to CTAC solution and was added into the solution with the same weight concentration as that of CTAC. The concentration of CTAC solution was chosen as 300 ppm. The viscosity of CTAC solution has a remarkable change compared with Newtonian fluid, and the difference of other physical properties can be negligible. So the viscosity was measured by a stress-controlled rotational rheometer (Kinexus Pro, Malvern instruments, Malvern, UK). We measured the viscosity at the temperature of 30 °C, which was the same as the temperature of bulk fluid in the convection cell. The CTAC solution will lose the effectiveness at high temperature. When the solution temperature rises to 60 °C, CTAC solution will be completely ineffective. Therefore, the maximum temperature in the experiments was no more than 50 °C.

Figure 4 shows the viscosity of all solutions used in the experiment. The viscosity of Newtonian fluids did not change with the shear rate. The CTAC solution was shear-thinning fluid and its viscosity was larger than that of water. And the viscosity of CTAC solution decreased with the increasing shear rate and it changed obviously at low shear rate. In order to avoid the influence of solution viscosity in the shadowgraph experiment, the sucrose solution with 30% mass fraction was used as Newtonian fluid. A characteristic velocity was used to estimate the mean velocity in the convection, defined as $u = (\alpha g \Delta T H)^{1/2}$, with g being the gravitational acceleration, H – the height of the cell, ΔT – the temperature difference across the cell, and α – the thermal expansion coefficient. The shear rate of CTAC solution flow in RBC was estimated about 0.3 by calculating u. At this rate the viscosity of CTAC solution is similar to that of 30% sucrose solution, as shown in fig. 4. But water was used as Newtonian fluid in the PIV measurement.

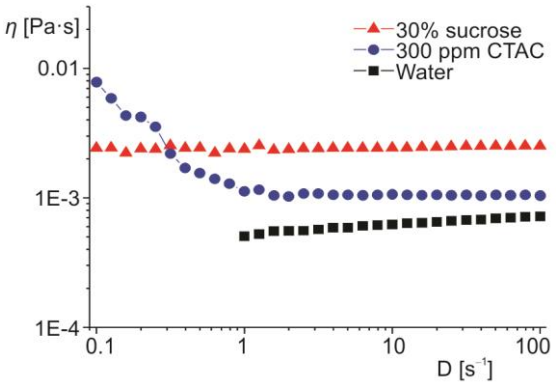

Figure 4. The viscosity vs. shear rate for all solutions

Results and discussion

Shadowgraph studies

The experiments recorded the plume motions from the beginning to the steady-state of convection. At first, the temperature difference between top plate and bottom plate was very small, so the system held in the thermal conduction state. With the temperature increase of bottom plate, hot plumes appeared and the system entered into thermal convection state. Hot plumes moved straight up in the cell in the beginning. When the average temperature in the cell was higher than that of top plate, cold plumes would appear. Large amounts of plumes moved up and down in the bulk and interacted with each other so as to induce the tilting movement of plumes. Finally, the system would reach the steady-state going through enough time, that is, most plumes moved regularly and formed LSC.

Figure 5 shows the shadowgraph images at the beginning of convection for different cases. It is clearly seen that the size of plumes in 300 ppm CTAC solution case is larger than that in 30% sucrose solution case, while the number of plumes is less. Plumes appear in 30% sucrose solution case after 4.5 minutes of heating, while plumes appear in 300 ppm CTAC solution case after 7.1 minutes of heating. That is to say, there exists a delay of plumes generation for 300 ppm CTAC solution case at the start state. As is known, plumes need absorb enough energy to generate from the temperature boundary-layer near the plates. However, the elastic deformation of surfactant additives consumed some energy and the mean size of plumes in 300 ppm CTAC solution case was larger. Therefore, in 300 ppm CTAC solution case, larger plumes carried more heat and assimilated more energy so as to cause a delay of plumes generation.

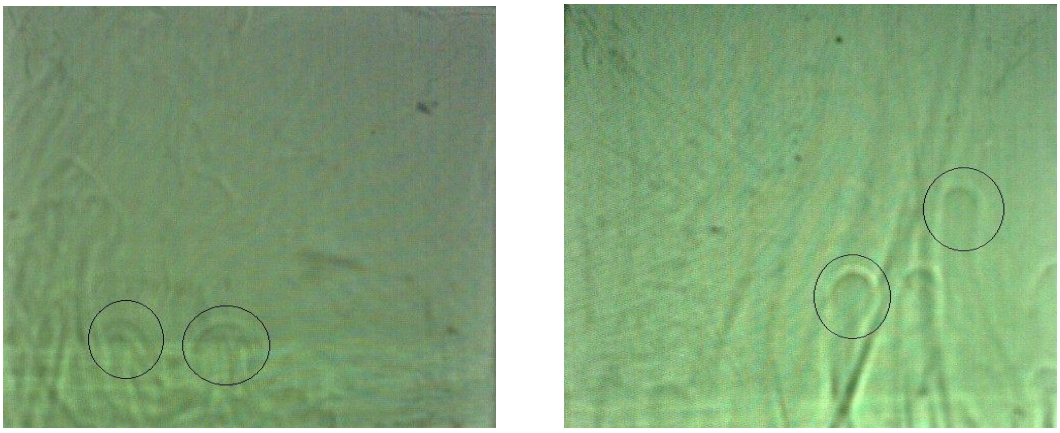

(a) **(b)**

Figure 5. The shadowgraph images of plumes motion for different cases at start stage; (a) 30% sucrose solution, 5 minutes 22 seconds, (b) 300 ppm CTAC solution, 9 minutes 15 seconds

Figure 6 gives the plume motions at steady-stage for different cases. It is found that LSC can be quickly formed in 30% sucrose solution case, but it does not form LSC in 300 ppm CTAC solution case during the experimental period. At the steady-stage, a large amount of plumes still remains moving straight when the experimental time reaches up to 20 hours. There are two reasons making it difficult to form LSC in 300 ppm CTAC solution case. One is that: the existence of elasticity in 300 ppm CTAC solution case absorbs some energy of

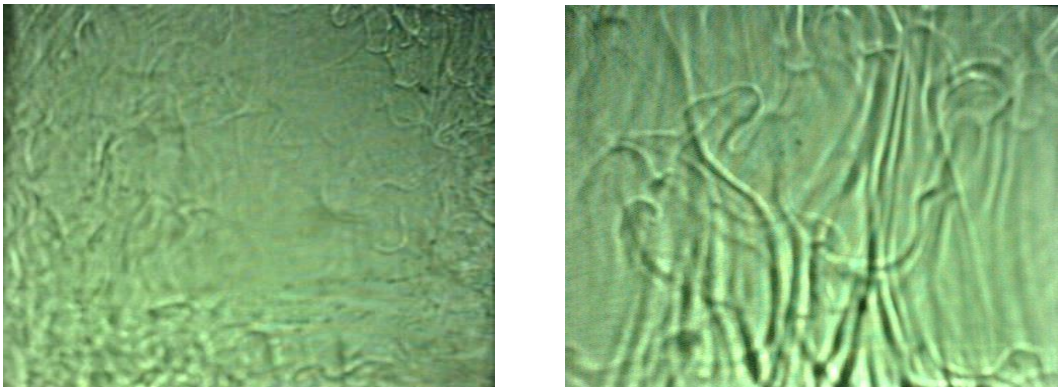

(a) **(b)**

Figure 6. The shadowgraph images of plumes motion for different cases at steady-stage; (a) 30% sucrose, (b) 300 ppm CTAC

plumes when they impact the plates, causing a decrease in the horizontal motion of plumes. The other is that: the shear-thinning characteristics of CTAC solution (as shown in fig. 4) makes the difference of viscosity between plumes areas and non-plumes areas, so the large viscosity of non-plumes areas hinder the interaction of plumes, so as to inhibit the horizontal motion of plumes.

Particle image velometry measurement

Keeping the same temperature difference between top plate and bottom plate, the velocity fields at the middle plane of the convection cell for different solutions were measured based on PIV. The control parameter in the experiment is the Rayleigh number Ra = $\alpha g \Delta T H^3/\nu\kappa$, with ν the kinetic viscosity and κ the thermal diffusivity. The kinetic viscosity in 300 ppm CTAC solution case was determined by the plume velocity measured with PIV. Figure 7 shows the mean velocity field for different cases. For water case, LSC is formed at the steady-state. There is one *flywheel* structure in the central region and two small-scale vortices in two corners. The large velocity is mainly concentrated in the sidewall area and it is small in the central region. With the increase of Rayleigh number, the velocity becomes larger. For 300 ppm CTAC solution case, it is clearly seen that LSC does not been formed although Rayleigh number reaches up to 10^8 orders of magnitude. This phenomenon is similar with that observed in the previous shadowgraph studies. And the velocity is much smaller than that in water case. The velocity in the horizontal direction is almost non-existent. From the distribution of velocity field, it is suggested again that it is difficult to form LSC in 300 ppm CTAC solution case.

In RBC flows, Nusselt number has been always used to reflect heat transfer, defined as: Nu = $JH/\chi\Delta T$, with J being the actual convective heat transfer and χ – the thermal conductivity. The J was got by the heating power of the power supply. Rayleigh number varied by changing the ΔT which is changed from 5 °C to 30 °C in the experiment. Due to the different viscosities of water and 300 ppm CTAC solution, Rayleigh number varied from $5.92\cdot10^8$ to $2.98\cdot10^9$ for water case and Rayleigh number varied from $1.70\cdot10^8$ to $9.30\cdot10^8$ for 300 ppm CTAC solution case. Figure 8 shows the relationship between Nusselt and Rayleigh numbers for different cases. Compared with that in water case at the same Rayleigh and Nusselt numbers for 300 ppm CTAC solution case has nearly 20% decrease. It can be clearly seen that the addition of surfactant leads to the reduction of heat transfer.

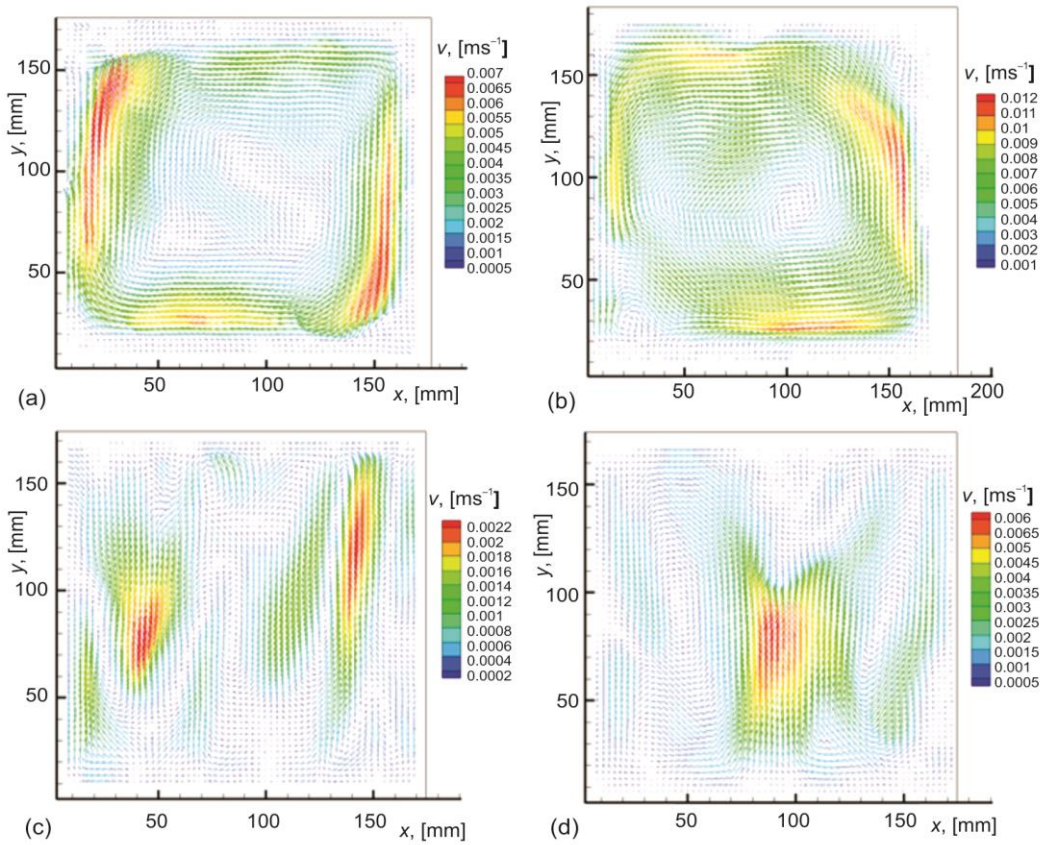

Figure 7. The mean velocity fields for different solutions; (a) water, Ra = $5.92 \cdot 10^8$, (b) water, Ra = $2.02 \cdot 10^9$, (c) 300 ppm CTAC solution, Ra = $1.71 \cdot 10^8$, and (d) 300 ppm CTAC solution, Ra = $7.84 \cdot 10^8$

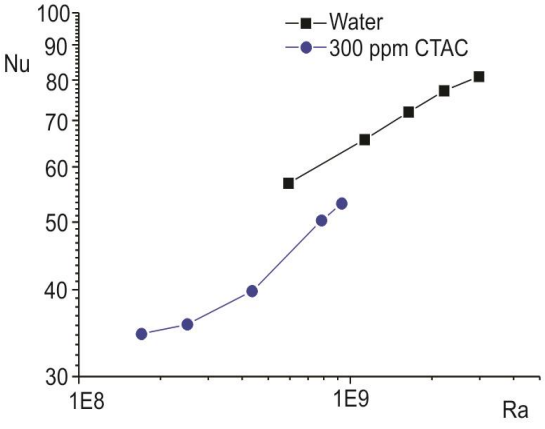

Figure 8. Nusselt *vs*. Rayleigh number for different solution cases

This phenomenon is owing to no formation of LSC in 300 ppm CTAC solution case. The previous phenomenon is similar with the results of RBC with polymer solutions in [17, 19, 22].

Conclusions

We experimentally studied the influence of surfactant additives on flow structures in turbulent Rayleigh-Benard convection. The CTAC solution was chosen as a kind of surfactant solutions. Shadowgraph visualization was used to visualize the motion of thermal plumes and PIV method was used to measure the velocity field in the whole convection cell.

The important conclusions are drawn as follows.

- There exists a delay of plumes generation for 300 ppm CTAC solution case at the start state and the size of plumes is larger.
- The LSC does not appear in 300 ppm CTAC solution although carrying out 20 hours for experiments. And the addition of surfactant inhibits the heat transfer in RBC.

Acknowledgment

This work was supported by the project of National Natural Science Foundation of China (No.51576051, 51606054). We also thank all members in the Complex Flow and Heat Transfer Laboratory of Harbin Institute of Technology.

Nomenclature

g – gravitational acceleration, [ms^{-2}]
H – height of the convection cell, [mm]
J – actual convective heat transfer, [Wm^{-2}]
Nu – Nusselt number, (= $JH/\chi\Delta T$), [–]
Ra – Rayleigh number, (= $\alpha g \Delta T H^3/\nu\kappa$), [–]
ΔT – temperature difference between top and bottom wall in the convection cell, [K]
u – characteristic velocity or the mean velocity in the convection cell, [ms^{-1}]

Greek symbols

α – thermal expansion coefficient, [K^{-1}]
κ – thermal diffusivity, [m^{2}s^{-1}]
ν – kinetic viscosity, [m^{2}s^{-1}]
χ – thermal conductivity, [Wm^{-1}K^{-1}]

References

[1] Xia, K. Q., Current Trends and Future Directions in Turbulent Thermal Convection, *Theoretical & Applied Mechanics Letters, 3* (2013), 5, pp. 1-12
[2] Moses, E., *et al*., An Experimental Study of Laminar Plumes, *Journal of Fluid Mechanics, 251* (1993), June, pp. 581-601
[3] Haramina, T., Tilgner, A., Coherent Structures in Boundary Layers of Rayleigh-Benard Convection, *Physical Review E, 99* (2004), No. 056306
[4] Zhou, Q., *et al*., Morphological Evolution of Thermal Plumes in Turbulent Rayleigh-Bénard Convection, *Physical Review Letters, 98* (2007), No. 074501
[5] Shang, X. D., *et al*., Measured Local Teat Transport in Turbulent Rayleigh-Bénard Convection, *Physical Review Letters, 90* (2003), No. 074501
[6] Shang, X. D., *et al*., Measurements of the Local Convective Heat Flux in Turbulent Rayleigh-Bénard Convection, *Physical Review E, 70* (2004), No. 026308
[7] Gasteuil, Y., *et al*., Lagrangian Temperature, Velocity, and Local Heat Flux Measurement in Rayleigh-Benard Convection, *Physical Review Letters, 99* (2007), No. 234302
[8] Kaczorowski, M., Wagner, C., Analysis of the Thermal Plumes in Turbulent Rayleigh- Benard Convection Based on Well-Resolved Numerical Simulations, *Journal of Fluid Mechanics, 618* (2009), Jan., pp. 89-112
[9] Zhou Q., Xia, K. Q., Physical and Geometrical Properties of Thermal Plumes in Turbulent Rayleigh-Bénard Convection, *New Journal of Physics, 12* (2010), No. 075006
[10] Krishnamurti, R., Howard, L. N., Large Scale Flow Generation in Turbulent Convection, *Applied Physical and Mathematical Sciences, 78* (1981), 4, pp. 1981-1985
[11] Qiu, X. L., Tong, P., Large-Scale Velocity Structures in Turbulent Thermal Convection, *Physical Review E, 64* (2001), No. 036304
[12] Xi, H. D., *et al*., From Laminar Plumes to Organized Flows: the Onset of Large-Scale Circulation in Turbulent Thermal Convection, *Journal of Fluid Mechanics, 503* (2004), Mar., pp. 47-56
[13] Brown, E., Ahlers, G., Rotations and Cessations of the Large-Scale Circulation in Turbulent Rayleigh-Bénard Convection, *Journal of Fluid Mechanics, 568* (2006), Dec., pp. 351-386
[14] Brown, E., *et al*., Reorientation of the Large-Scale Circulation in Turbulent Rayleigh-Bénard Convection, *Physical Review Letters, 95* (2005), No. 084503
[15] Xi, H. D., Xia, K. Q., Cessations and Reversals of the Large-Scale Circulation in Turbulent Thermal Convection, *Physical Review E, 75* (2007), No. 066307

[16] Xi, H. D., Xia, K. Q., Azimuthal Motion, Reorientation, Cessation and Reversal of the Large-scale Circulation in Turbulent Thermal Convection: a Comparison between Aspect Ratio One and One-Half Geometries, *Physical Review E*, *78* (2008), No. 036306
[17] Ahlers, G., Nikolaenko, A., Effect of a Polymer Additive on Heat Transport in Turbulent Rayleigh-Benard Convection, *Physical Review Letters*, *104* (2010), No. 034503
[18] Benzi, R., *et al*., Effect of Polymer Additives on Heat Transport in Turbulent Thermal Convection, *Physical Review Letters*, *104* (2010), No. 024502
[19] Wei, P., *et al*., Enhanced and Reduced Heat Transport in Turbulent Thermal Convection with Polymer Additives, *Physical Review E*, *86* (2012), No. 016325
[20] Dubief, Y., Heat Transfer Enhancement and Reduction by Polymer Additives in Turbulent Rayleigh-Bénard Convection, On-line first, *arXiv preprint arXiv*, 1009.0493, 2010
[21] Demir, H, Rayleigh-Bénard Convection of Viscoelastic Fluid, *Applied Mathematics and Computation*, *136* (2003), 2-3, pp. 251-267
[22] Chen, J.P., *et al*., Effect of Polymer Additives on Heat Transport and Large-Scale Circulation in Turbulent Rayleigh-Benard Convection, *Physical Review E*, *96* (2017), No. 013111

Paper submitted: October 26, 2017
Paper revised: November 23, 2017
Paper accepted: November 23, 2017